JCIM JOURNAL OF CHEMICAL INFORMATION AND MODELING

Cite This: J. Chem. Inf. Model. XXXX, XXX, XXX−XXX

Article

pubs.acs.org/jcim

Molecular Dynamics Simulations Revealed the Regulation of Ligands to the Interactions between Androgen Receptor and Its Coactivator

Na Liu,[†,‡,⊥] Wenfang Zhou,[§,⊥] Yue Guo,[†,‡] Junmei Wang,[∥] Weitao Fu,[§] Huiyong Sun,[§] Dan Li,[§] Mojie Duan,*[,†] and Tingjun Hou*[,§]

[†]Key Laboratory of Magnetic Resonance in Biological Systems, State Key Laboratory of Magnetic Resonance and Atomic and Molecular Physics, National Center for Magnetic Resonance in Wuhan, Wuhan Institute of Physics and Mathematics, Chinese Academy of Sciences, Wuhan 430071, China

[‡]University of Chinese Academy of Sciences, Beijing 100049, People's Republic of China

[§]College of Pharmaceutical Sciences, Zhejiang University, Hangzhou, Zhejiang 310058, People's Republic of China

[∥]Department of Pharmaceutical Sciences, University of Pittsburgh, Pittsburgh, Pennsylvania 15261, United States

Supporting Information

ABSTRACT: The androgen receptor (AR) plays important roles in gene expression regulation, sexual phenotype maintenance, and prostate cancer (PCa) development. The communications between the AR ligand-binding domain (LBD) and its coactivator are critical to the activation of AR. It is still unclear how the ligand binding would affect the AR−coactivator interactions. In this work, the effects of the ligand binding on the AR−coactivator communications were explored by molecular dynamics (MD) simulations. The results showed that the ligand binding regulates the residue interactions in the function site AF-2. The ligand-to-coactivator allosteric pathway, which involves the coactivator, helix 3 (H3), helix 4 (H4), the loop between H3 and H4 (L3), and helix 12 (H12), and ligands, was characterized. In addition, the interactions of residues on the function site BF-3, especially on the boundary of AF-2 and BF-3, are also affected by the ligands. The MM/GBSA free energy calculations demonstrated that the binding affinity between the coactivator and apo-AR is roughly weaker than those between the coactivator and antagonistic ARs but stronger than those between the coactivator and agonistic ARs. The results indicated that the long-range electrostatic interactions and the conformational entropies are the main factors affecting the binding free energies. In addition, the F876L mutation on AR-LBD affects the ligand-to-coactivator allosteric pathway, which could be the reason for point mutation induced tolerance for the antagonistic drugs such as enzalutamide. Our study would help to develop novel drug candidates against PCa.

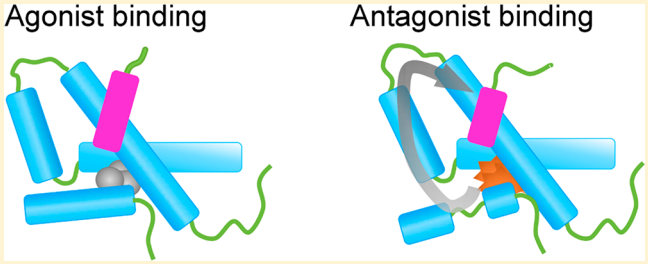

INTRODUCTION

The androgen receptor (AR) is activated by the binding of androgenic hormones, testosterone, or dihydrotestosterone (DHT). AR takes part in the regulation of expression of many important genes, which are critical for the development and maintenance of the male sexual phenotype in healthy people.[1] However, AR promotes the proliferation of cancer cells in prostate cancer (PCa) patients.[2−4] Inhibiting the activation of AR by antagonistic drugs has been regarded as a promising way to treat PCa.[5,6]

As a member of the nuclear receptors (NRs) family, the transcriptional activity of AR depends on the recruitment of steroid receptor coactivators (SRCs) to its ligand binding domain (LBD).[7,8] The unique coactivators recruited by AR contain the aromatic-rich motif (FXXLF) instead of the leucine-rich motif (LXXLL) for most other NRs.[9,10] Accumulated evidence showed that the transcriptional activity of AR, which is crucially important in the development of PCa, would be inhibited by breaking the AR−coactivator interactions.[11−13] Understanding the detailed molecular mechanism of AR−coactivator interactions would provide deeper pharmacological insights into the development of therapies for the treatment of PCa.

The short hydrophobic residue-rich motif of coactivators interacts with the so-called activation function (AF-2) region within the AR-LBD.[14] AF-2 is a hydrophobic groove on the surface of the AR-LBD that is formed by a number of residues in helices 3, 4, and 12 (Figure 1A and B).[15,16] The structure of AF-2 is regulated by the binding of ligands to AR. For instance, the binding of agonistic AR ligands, such as dihydrotestosterone and methyltrienolone (R1881), would induce the formation of a suitable conformation on the AF-2 region for the

Received: May 12, 2018
Published: July 11, 2018

DOI: 10.1021/acs.jcim.8b00283
J. Chem. Inf. Model. XXXX, XXX, XXX−XXX

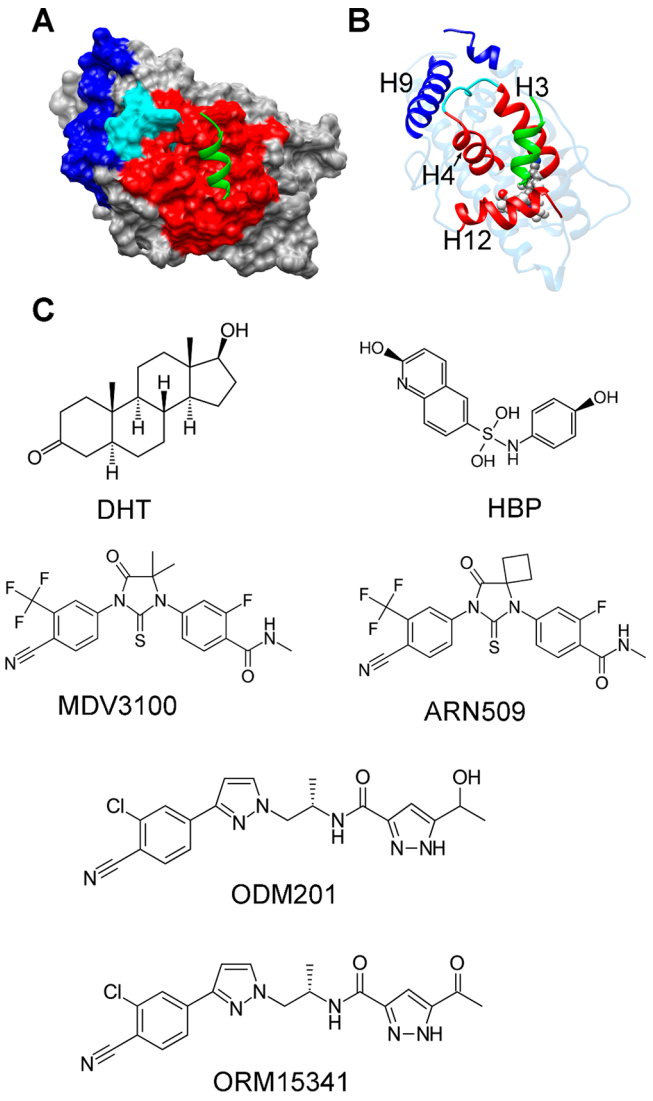

Figure 1. (A) The crystallographic structure of AR in complex with the coactivator peptide (PDB ID: 3V49[34]). AR is represented by surface and the coactivator is represented by green ribbon. The AF-2 groove on AR is colored in red. The BF-3 groove is colored in blue, and the boundary between AF-2 and BF-3 is colored in cyan. (B) The same structure in A but shown in ribbon. (C) The chemical structures of the ligands studied in this work.

recruitment of coactivators and amplifying the activity of AR.[17,18] On the other side, the binding of AR antagonistic drugs, such as flutamide, bicalutamide, and the second generation anti-androgen drug enzalutamide (MDV3100), to the AR LBD on the similar binding site for agonists would induce AF-2 to form a different conformation compared with the agonist-bound ARs.[19−21]

Plenty of studies demonstrated that ligands would modulate the stability and integrity of H12.[22−25] H12 takes part in the formation of the AF-2 groove after the structural rearrangement induced by the hormone binding, which provides a molecular mechanism for the regulation between ligands and AR coactivators.[26] However, there still remain many unsolved problems. For instance, while the FXXFL motif of coactivators mainly interacts with H3 and H4 of AF-2 according to the X-ray crystallographic structures (Figure 1), how does the structural change of H12 induced by ligand-binding affect the interactions between coactivators and AR? In addition to the AF-2 site, the BF-3 function site was found to be important for the activity of AR.[27,28] Are there any communications between AF-2 and BF-3? In addition, some single mutations on the AR-LBD would convert antagonistic ligands into agonists and therefore confer drug resistance, e.g., the drug tolerance induced by the T877A mutation to hydroxyflutamide (HFT) and the F876L mutation to enzalutamide (MDV3100).[29,30] What if the antagonist−agonist conversions are also related to the AR-coactivator interactions? Until now, computational studies have made great efforts to understand the molecular mechanisms of AR-ligand recognition and AR activity. For instance, Xu et al. proposed that the DHT binding would increase the stability of the ligand binding pocket and the structure of LBD.[31] Osguthorpe and Hagler studied the antagonistic mechanism of bicalutamide (Bcu) based on molecular dynamics (MD) simulations and quantum mechanical (QM) calculations.[32] By combining with MD simulations and mutation experiments, Korpal et al. found that the benzamide motif of enzalutamide extends away from H12 if F876 is mutated to a small leucine based on the computational docking models.[29] Liu et al. demonstrated that the interactions between the C-ring of enzalutamide and H12 play important roles in the transcription activity of AR by simulating the wild-type (WT) AR and its mutants.[33] Although progress has been achieved, the detailed mechanism about how the agonistic/antagonistic ligands regulate the AR-coactivator communications still remains unclear.

In this study, a series of microsecond-long MD simulations was performed on the AR-LBDs in complex with a coactivator peptide, including the apo-AR-LBD without a ligand, the AR-LBDs with two agonistic ligands (DHT and HBP), and the AR-LBDs with four antagonistic ligands (MDV3100, ODM201, ARN509, and ORM15341). The simulations revealed that the ligand binding would regulate the interactions between the AR AF-2 groove and the coactivator motif; i.e., the binding of agonistic ligands would facilitate the AF-2/coactivator interactions, and the antagonistic ligands would depress such interactions. Further analyses show that the allosteric regulation of ligands to the coactivator binding obeys the ligand−H12-H3/H4-coactivator pathway. The antagonist-to-agonist conversions of the ligands MDV3100 and ODM201 by single mutants were also modulated by the above allosteric pathway. In addition, the quantitative binding free energies between the coactivator and different AR-LBD systems were calculated by Molecular Mechanics/Generalized Born Surface Area (MM/GBSA). Our results revealed the detailed mechanism of how ligands regulate the coactivator recruitment of AR and provided clues to rational pharmacological intervention to inhibit the activity of AR.

METHODS

Ligands Docking and Initial Structure Models. MD simulations were performed on a total of 11 systems, including seven WT AR-LBD systems, including the apo-AR-LBD without ligand, the AR-LBD bound with an agonistic ligand (DHT or HBP), and the AR-LBD bound with an antagonistic ligand (MDV3100, ODM201, ARN509, or ORM15341), and four AR mutants, including the F876L mutated AR-LBD bound with MDV3100, the T877A mutated AR-LBD bound with MDV3100, the F876L mutated AR-LBD bound with ODM201, and the T877A mutated AR-LBD bound with ODM201. The human WT AR-LBD in complex with a selective androgen receptor modulator PK0950 and an AR coactivator peptide (GAFQNLFQSVR) were selected as the initial template in the following molecular docking calculations (PDB entry: 3V49[34]). The initial structures

DOI: 10.1021/acs.jcim.8b00283
J. Chem. Inf. Model. XXXX, XXX, XXX−XXX

for MD simulation were generated by the *Glide* module[35] implemented in Schrödinger 9.0. F876L/T877A mutants of AR-LBD were established and optimized through the *Build and Edit Protein* module in Discovery Studio 2.5. For the protein structures, the *Protein Preparation Wizard*[36] in Schrödinger 9.0 was used to remove crystallographic waters, ions, and DTT; add hydrogens; fix bond orders; assign partial charges with the OPLS force field; and minimize the structures until the root-mean-square deviation (RMSD) reached a maximum value of 0.3 Å. The structures of all ligands were processed by using the *LigPrep* module in Schrodinger 9.0. For each compound, the ionized states were generated by using *Epik* at pH = 7.0 ± 2.0. For each protein, a binding box with a size of 10 Å × 10 Å × 10 Å centered on the cocrystallized ligand was generated by using the *Receptor Grid Generation* component of *Glide*. The van der Waals radius scaling factor and the partial atomic charge cutoff were set to 1.0 and 0.25, respectively. All the prepared structures of all six ligands were docked into the WT or F876L/T877A mutated AR-LBD and scored by the extra precision (XP) scoring mode. The binding pose with the best docking score for each molecule was chosen for the following simulations. The above docking strategy was validated by redocking PK0950 into the crystallographic structure. The redocking RMSD of the ligand is 0.32 Å, which demonstrated the high reliability of the docking scheme we used.

MD Simulation Protocols. The AMBER99SB-ILDN force field[37] and the general amber force field (gaff)[38] were used for the proteins and ligands, respectively. The TIP3P water molecules were added as the solvent and the solute atoms were at least 12 Å away from the boundary of the rectangular box. The counterions, i.e., chlorine atoms, were added to neutralize the net charge of each system. The long-range electrostatic interactions were handled by the particle mesh Ewald (PME) algorithm,[39] and the nonbonded cutoff for the real-space interactions was set to 10 Å. A hybrid protocol of the steepest descent method and the conjugate gradient method was employed to do the minimization. Ten-thousand steps of steepest descent minimization with the restraint (a force constant of 100 kcal/mol·Å^2) on the protein and ligand were first performed, and then the conjugate gradient method without any restraint was used until a maximum 20 000 iteration steps was reached or the convergence criterion (the root-mean-square of the energy gradient is less than 1.0 × 10^{-4} kcal/mol·Å) was satisfied. The systems were heated up from 0 to 300 K linearly over a time period of 100 ps with the restraint (force constant of 10 kcal/mol·Å^2) on the solute in the NVT ensemble, and then the systems were equilibrated without restraint for 1 ns with a Langevin thermostat[40] in the NPT (P = 1 atm and T = 300 K) ensemble. Finally, the 1-μs production runs were carried out with CUDA-version Amber14[41] in the NPT (P = 1 atm and T = 300 K) ensemble. The SHAKE algorithm[42] was used to restrain the covalent bonds between heavy atoms and hydrogen atoms, and the time step was set to 2 fs. The snapshots were saved every 20 ps, and the conformations in the last 200 ns trajectories were used in the following analysis if there was no additional annotation. The RMSDs as a function of simulation time for the AR bound with coactivator, AF-2 bound with coactivator, and ligand were given in Figures S1, S2, and S3, respectively. The RMSDs are well converged in the latter part of all the simulations, and the RMSD fluctuations in the last 200 ns are less than 1 Å.

Fraction of Native Contact Analysis. The fraction of native contacts (Q) analysis[43] was employed to evaluate the differences of residue interactions in the query structures to a given structure, which is usually the native structure, i.e., the X-ray or NMR experimental structure. For the residues that are more than three residues apart in sequence, their heavy atoms (each from a different residue) are considered to be in contact with each other if the distance between the atoms is less than 4.5 Å. The total number of heavy-atom pairs that are in contact in the native state is N in eq 1. The fraction of the native contacts for a given snapshot S is defined as[43]

$$Q(S) = \frac{1}{N}\sum_{(i,j)} \frac{1}{1 + \exp[\beta(r_{ij}(S) - \lambda r_{ij}^0)]} \quad (1)$$

where r_{ij}^0 is the distance between heavy atoms i and j in the native structure and $r_{ij}(S)$ is the distance between the same atom pair in snapshot S. The smoothing parameter β is set to 5 Å^{-1}, and the contact fluctuation is taken into account by the parameter λ = 1.8. The summation runs over the N pairs. The definition of fraction of native contacts for residue k in snapshot S is similar to Q for the whole protein,[44] but only the contacts associated with residue k are calculated:

$$Q_k(S) = \frac{1}{N_k}\sum_{(k,j)} \frac{1}{1 + \exp[\beta(r_{kj}(S) - \lambda r_{kj}^0)]} \quad (2)$$

where N_k is the number of heavy-atom pairs in native contact between residues k and other residues (>3 residues apart in sequence). If there is no heavy atom within 4.5 Å to the heavy atoms of residue k in the native structure, then $Q_k(S) = 0$.

Binding Free Energy Calculation. The binding free energy between the coactivator and the AR-LBD was calculated by the MM/GBSA approach:[45]

$$\Delta G_{\text{bind}} = G_{\text{com}} - (G_{\text{AR}} + G_{\text{coact}}) \quad (3)$$

$$\Delta G_{\text{bind}} = \Delta H - T\cdot\Delta S \approx \Delta E_{\text{MM}} + \Delta G_{\text{solv}} - T\cdot\Delta S \quad (4)$$

$$\Delta E_{\text{MM}} = \Delta E_{\text{int}} + \Delta E_{\text{vdw}} + \Delta E_{\text{ele}} \quad (5)$$

$$\Delta G_{\text{solv}} = \Delta G_{\text{GB}} + \Delta G_{\text{SA}} \quad (6)$$

where ΔE_{int} (intramolecular interactions, including bond, angle, and dihedral energies) in eq 5 can be completely canceled because the single trajectory strategy was used for the MM/GBSA calculations. The nonpolar part of the solvation free energy (ΔG_{SA}) was calculated by the solvent-accessible surface area (SASA) through the LCPO algorithm:[46] $\Delta G_{\text{SA}} = \gamma \times \text{SASA} + \beta$, where the surface tension constants γ and β were set to 0.0072 and 0, respectively. The polar part of the solvation energy (ΔG_{GB}) was estimated using the Generalized Born (GB) model proposed by Onufriev et al. (GB$^{\text{OBC1}}$, igb = 2).[47] The interior and exterior dielectric constants were set to 4 and 80, respectively. The ΔE_{vdw}, ΔE_{ele}, ΔG_{GB}, and ΔG_{SA} terms were computed based on the 2000 snapshots extracted from the last 200 ns MD trajectories. However, due to the expensive computational cost of normal-mode analysis (NMA), 50 snapshots evenly extracted from the last 200 ns MD trajectories were used to calculate the conformational entropies with the *MMPBSA.py*[48] module in Amber14.

RESULTS AND DISCUSSION

Ligand Binding Regulates the Configurations of AF-2 and Coactivator. The formation of a special configuration of the functional AF-2 region is necessary for the activation of AR. It was proposed that the binding of antagonistic ligands might block the interactions between the AF-2 function site

DOI: 10.1021/acs.jcim.8b00283
J. Chem. Inf. Model. XXXX, XXX, XXX−XXX

and coactivators.[9] The detailed structural changes of AF-2 induced by different ligands were demonstrated by the simulations in this study. As shown in Figure 2, the representative structures

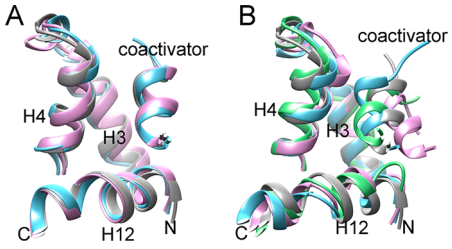

Figure 2. Comparisons of the AF-2 grooves and coactivators between the simulated structures and experimental structure. The conformations in the last 200 ns trajectories were classified into structure clusters based on the heavy-atom RMSDs. The AF-2 structures of the largest cluster center were selected as the representative structures. (A) Structure overlap of AF-2 bound with agonistic ligands (DHT, colored in cyan; HBP, colored in magenta) against the X-ray structure (colored in gray). (B) Structural overlap of AF-2 of the ODM201 bound AR (colored in cyan), MDV3100 bound AR (colored in magenta), and apo-AR (colored in green) against the X-ray structure (colored in gray). The N- and C-terminus of H12 were labeled.

of AF-2 in the different ligand bound ARs were overlapped with the X-ray crystallographic structure (PDB ID: 3V49). The agonistic ligand (DHT and HBP) bound structures are given in Figure 2A, and the antagonistic ligand (MDV3100 and ODM201) bound ARs and the AR without ligand binding are given in Figure 2B. The structures of the AF-2 region of the agonistic ligand bound ARs are basically identical to that of the X-ray structure, which would facilitate the binding of coactivators (Figure 2A). On the other hand, there are many differences on the AF-2 scaffold structure of the inactivate ARs compared with that of the X-ray structure; for instance, the breaking of the helix structure on the middle of H12 changes the orientation of the C-terminus of H12. In addition, the loop region between H3 and H4 shifts away from the position in the X-ray structure (Figure 2B).

Compared with the experimental structure, the overall RMSDs of the agonistic ARs are less than 3 Å, and those of the AF-2 regions in the DHT- and HBP-bound ARs are around 2 Å during the simulations (Figure 3). However, the AF-2

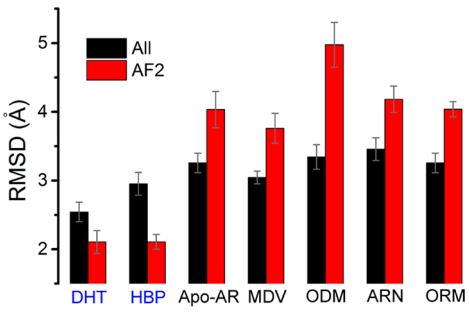

Figure 3. Overall RMSD and AF2 RMSD. The overall RMSD considered all the heavy atoms on AR-LBD and its coactivator except the 10 N-terminal residues. The AF2 RMSD took into account the residues 709−741 (H3−H4), 892−907 (H12), and the coactivator peptide. The average RMSD values were calculated over the last 200 ns trajectories. The error bars give the errors during the last 200 ns simulations. The labels of the agonistic ARs were colored in blue. The crystallographic structure (PDB ID: 3V49[34]) was used as the reference structure.

RMSDs of the antagonistic ARs are around 4 Å (Figure 3), which demonstrates the structural changes of AF-2 on ARs bound with antagonistic ligands during the simulations. The rearrangement of the C-terminus of H3, H4, and H12 altered the surface of the AF-2 groove, which might reduce the coactivator recruitment ability. As shown in Figure 2B, the helical structures in the C-terminus of coactivators unfolded, and the coactivators preferred to depart from the ARs in the antagonistic ARs during the simulations. In fact, the modulation of the coactivator binding might be a common feature in the nuclear receptors; for instance, it was revealed that many ligands have the ability to inhibit the binding affinity of coactivator peptides to the estrogen receptor (ER)[49] or vitamin D receptor (VDR).[50]

Ligands Regulate the Residue Interactions in AF-2. The fraction of native contact (Q) was widely used in protein folding studies and protein structure analysis. The Q value calculates the residue contact score in the given conformation compared with a specific structure, i.e., the native structure (eq 1).[43] And the fraction of residue native contact Q_k characterizes the native-ness of residues in the dynamic conformations (eq 2).[44] In this study, the X-ray structure of the agonistic AR (PDB id: 3V49) was used as the native structure, and the fraction of residue native contacts (Q_k) was calculated to show the residue interaction properties in different ligand-bound ARs. Figure 4

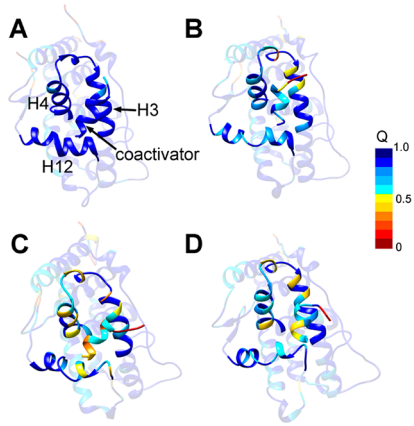

Figure 4. Fraction of the native contact for the residues on various ligand bound AR. (A) AR bound with DHT; (B) Apo-AR; (C) AR bound with ODM201; (D) AR bound with MDV3100. To highlight the AF-2 groove (C-terminus of H3, H4 and H12) and the coactivator, the other regions were transposed. The color scale of $\langle Q_k \rangle$ values is shown.

gave the $\langle Q_k \rangle$ on the residues of DHT-AR, apo-AR, ODM201-AR, and MDV3100-AR, respectively. The angle bracket means the average value over the conformations of the simulations. The range of $\langle Q_k \rangle$ is from 0 to 1. $\langle Q_k \rangle = 1$ means that the residue k in the simulated structure has an identical residue-interaction relationship with the corresponding residue in the X-ray structure. On the other side, $\langle Q_k \rangle = 0$ means that the native contacts are totally lost during the simulations for the residue k. In Figure 4, the residues were colored based on their Q values; i.e., the residues with small $\langle Q_k \rangle$ were colored in red, and the residues with large Q were colored in blue. For the agonistic form DHT-AR (Figure 4A), most residues have the $\langle Q_k \rangle$ values close to 1, suggesting that the structure and the residue interactions for the agonistic AR during the simulations were similar to those for the crystallographic structure. However, many of the residues in the antagonistic ARs have very low $\langle Q_k \rangle$ (Figure 4C and D). The low Q_k residues are mainly located on

DOI: 10.1021/acs.jcim.8b00283
J. Chem. Inf. Model. XXXX, XXX, XXX−XXX

H3, L3 (the loop linking H3 and H4), H4, and H12 (Figure 4 and Figure S4). Since the AF-2 groove is consisted by H3, H4, and H12, the analysis of the Q values demonstrated that the ligand-binding greatly influences the residue interactions on the AF-2 region.

The residues which have low $\langle Q_k \rangle$ values in the antagonistic AR and high $\langle Q_k \rangle$ values in the agonistic AR are listed in Figure S5, i.e., the residues 716, 717, and 720 on H3; 726−729 on L3; 731, 732, 734, and 738 on H4; 752 on H5; 823 and 826 on H9; and 891, 894, 897, and 898 on H12. As an example, Figure 5 gave the interactions of the residue K720 in different

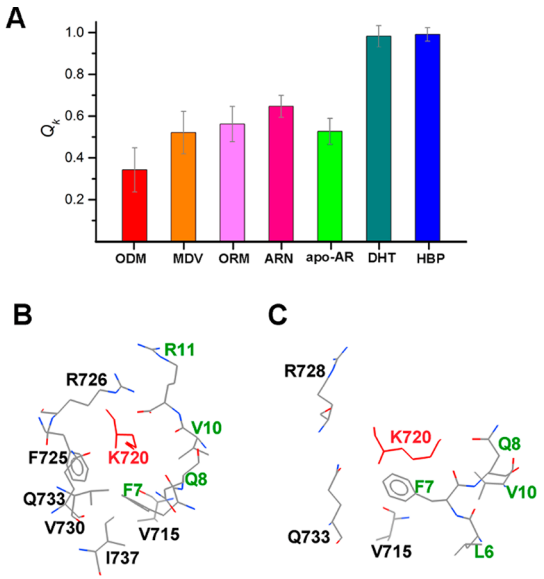

Figure 5. Residue interactions of the residue K720. (A) $\langle Q_k \rangle$ values of K720 in different ligand-bound ARs. (B) The residue interactions K720 in the DHT-bound AR. (C) The residue interactions K720 in the ODM201-bound AR. In B and C, only long-range interactions (the sequence interval with K720 larger than 3) were given. The residue names and numbers were labeled. K720 was colored in red, and residues in the coactivator were colored in green.

ligand bound ARs. K720 was proved to be a critical residue to the FXXLF coactivator peptide binding based on different experimental evidence.[51−53] The $\langle Q_k \rangle$ values of K720 are around 0.5 on the nonactive ARs, i.e., the apo-AR or AR bound with the antagonistic ligands (Figure 5A). In the DHT-bound agonistic AR, K720 was buried by the residues V715, F725, R726, V730, Q733, and I737 on the AR-LBD and the residues on the coactivator (Figure 5B). However, most of the contacts with K720 were lost in the ODM201-bound antagonistic AR, and K720 was exposed to the solvent (Figure 5C).

The residues with a large $\langle Q_k \rangle$ difference in the agonistic/antagonistic ARs revealed by our study might be critical to the activity of AR. Actually, our observations are consistent with the *in vitro* experimental transcriptional assays, which demonstrated that the single mutations of the residues 726, 727, and 826 would affect the transactivation activity or N-terminus and C-terminus communications of AR.[54] To further demonstrate the importance of residues with larger $\langle Q_k \rangle$ differences, we analyzed the residue conservation of the nuclear receptor family. The conserved residues are usually critical in the evolution to maintain the overall structures and functions of proteins. We aligned the sequence of the AR-LBD to those of other nuclear receptors, including the estrogen receptor (ER), glucocorticoid receptor (GR), mineralocorticoid receptor (MR), and progesterone receptor (PR). The results show that most of the residues with large $\langle Q_k \rangle$ differences are conserved in these proteins (Figure S6). For instance, as shown in Figure 5, the Q_k difference for residue 720 between the antagonistic ARs and agonistic ARs is larger than 0.4; meanwhile, all the residues are lysine on the positions corresponding to residue 720 in AR for all four of the other nuclear receptors. The conserved residues with large $\langle Q_k \rangle$ differences show their importance to the activity of the AR functions and might be potential target sites to design new antiandrogen drugs.

BF-3 Function Site Regulated by Ligand Binding. BF-3 is another important protein−protein interaction site on the AR-LBD. Although only some small compounds were found to bind with BF-3, research suggested its modulating role in AR activity by interacting with other proteins.[27] BF-3 is adjacent to AF-2, which consists of helix 1, helix 9, and L3 loop. L3 loop is the boundary between BF-3 and AF-2 and links H3 and H4. Functional assays show that mutations on many residues on BF-3 would affect the AR functions. We found that the ligand-binding might not change the overall structure and backbone configuration of the BF-3 site, and the helical structures on H9 were also observed in the antagonistic ARs. Nevertheless, the binding of antagonistic ligands would significantly affect the side-chain orientations and residue interactions of many residues in this region, especially on L3 loop. As shown in Figure S5, the $\langle Q_k \rangle$ differences for residues 726 and 727 in the agonistic and antagonistic ARs are around 0.4. In addition, the $\langle Q_k \rangle$ values for the residues 823 and 829 on H9 in the antagonistic ARs are slightly lower (about 0.2) than those in the agonistic ARs. The orientation changes of the charged residues and hydrophobic residues might reduce the interaction of AR to other proteins and inhibit the activity of AR.

Allosteric Regulation Pathway from Ligands to Coactivators. In our previous work, we demonstrated that the residues W741 and H874 play critical roles in the communication between ligands and AR-H12.[25] The binding of antagonistic ligands would destabilize the structure of H12. In this study, our simulations further demonstrated the damaging of H12 integrality by the antagonistic ligands (Figure 2B). In addition, the allosteric mechanism between the ligands and the coactivator was uncovered. We found that the allosteric regulation follows the following pathway. (1) The structures of H12 were regulated by the binding of ligands. For the agonistic ligands, H12 was stabilized to be a good α-helix. For the antagonistic ligands or apo-AR, the C-terminus of H12 would move away from the ligands. (2) The orientations of the residues Q902 and K905 were regulated by the arrangement of H12. In the agonistic AR, the residues Q902 and K905 form an interaction network with the polar/charged residues Q738 and W739 on the C-terminal of H5 and stabilize the structure of H5 (Figure 6A). However, in the antagonistic AR or apo-AR, the interactions between H5 and H12 were decreased due to the unstable structure of H12 (Figure 6B). (3) The increasing or decreasing of the interactions between residues on H12 and H5 would destabilize the structures of H4/H5. (4) The interactions between AF-2 and the coactivator are controlled by the structures of H5 and H12. For the agonistic ARs, AF-2 contacts with the coactivator via the hydrophobic interactions between residues AR-F725/AR-I737 and F7/F3 on the coactivator motif, as well as the hydrogen bond between the K720 side chain and K10 backbone on the coactivator motif (Figure 6A). However, the change of the AF-2 surface induced by antagonistic ligands would reduce the

DOI: 10.1021/acs.jcim.8b00283
J. Chem. Inf. Model. XXXX, XXX, XXX−XXX

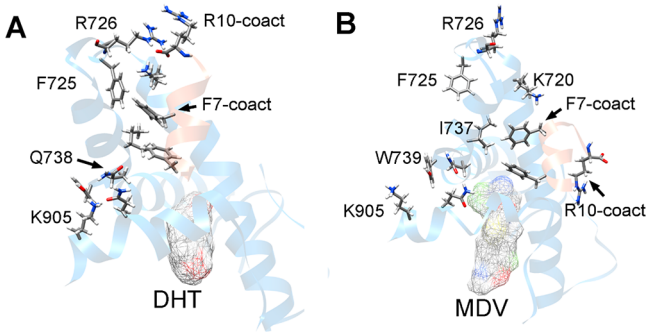

Figure 6. Allosteric pathway between ligand and coactivator. (A) The residue interactions in the allosteric pathway from DHT to the coactivator. (B) The allosteric pathway between the MDV3100 and coactivator. The ligand-binding pocket and AF-2 with the coactivator are shown as a ribbon. The ligands are represented by the meshed surface. ARs are colored in blue, and coactivators are colored in orange. Some important residues are labeled and shown as sticks. The conformations in the last 200 ns trajectories were classified into structure clusters based on the heavy-atom RMSDs. The AF-2 structures of the largest cluster center were selected as the representative structures.

above hydrophobic interactions (Figure 6B), which might be the reason for the unfavorable binding between the antagonistic AR and coactivators.

Coactivator-AR Binding Energy Influenced by Ligand Binding. The binding of antagonistic ligands decreased the interactions between residues in the AR-LBD and the C-terminus of its coactivator. Therefore, the residues in the coactivator, especially its C-terminus, depart from the AF-2 groove in the inactivated AR. To investigate the energetic implication between the AR and coactivator, the MM/GBSA analyses were performed on the MD trajectories. MM/GBSA was proved to be a powerful tool in the prediction of protein−ligand or protein−peptide binding free energies. In addition, the normal model analysis (NMA) technology was employed to calculate the entropy effects and characterize the contributions of the AR/coactivator fluctuation to binding free energies. The MM/GBSA and NMA calculation results are summarized in Table 1. In general, the binding free energies between the coactivator and agonistic ARs are lower than those between the coactivator and antagonistic ligands and those between the coactivator and apo-AR. The binding free energy between the coactivator and apo-AR was used as the reference, and the difference of the binding free energies ($\Delta\Delta G_{binding}$) is also listed in Table 1. It can be seen that the $\Delta\Delta G_{binding}$ values are negative for the agonistic ARs (−1.4 kcal/mol for DHT-binding AR and −3.0 kcal/mol for HBP-binding AR), suggesting that the binding of agonistic ligands would promote the interaction between AR and its coactivator. On the other hand, all the antagonistic ARs have positive $\Delta\Delta G_{binding}$ values. Both the enthalpies and entropies contribute to the binding between the coactivator and ARs, though the entropies might have larger effects on the energy differences. Basically, the potential energy differences for the coactivator binding to the antagonistic ARs or the agonistic ARs come from the electrostatic interactions (ΔE_{ele} are around −60 kcal/mol for the binding of the coactivators to the agonistic ARs, which are much lower than those for the binding of the coactivators to the antagonistic ARs). In addition, the coactivators bound to the agonistic ARs have much higher solvation free energies (ΔG_{GB}). The results indicate that the long-range electrostatic interactions might be critically important to the interactions

Table 1. Binding Free Energies (Units in kcal/mol) between the Coactivators and AR-LBDs

	ODM_WT	MDV_WT	ORM_WT	ARN_WT	DHT_WT	HBP_WT	ODM_F876L	ODM_T877A	MDV_F876L	MDV_T877A	Apo-AR
ΔE_{vdw}	−51.5 ± 51.	−50.1 ± 50.	−51.9 ± 51.	−52.9 ± 52.	−52.8 ± 52.	−52.0 ± 52.	−51.2 ± 51.	−49.7 ± 49.	−54.9 ± 54.	−51.0 ± 51.	−47.2 ± 47.
ΔE_{ele}	−55.9 ± 55.	−55.4 ± 55.	−50.6 ± 50.	−51.7 ± 51.	−57.4 ± 57.	−60.6 ± 60.	−56.1 ± 56.	−50.6 ± 50.	−59.2 ± 59.	−55.9 ± 55.	−52.1 ± 52.
ΔG_{GB}	57.7 ± 7.7	56.4 ± 6.4	53.3 ± 3.3	54.7 ± 4.7	59.7 ± 9.7	61.4 ± 1.4	57.8 ± 7.8	52.9 ± 2.9	61.9 ± 1.9	57.2 ± 7.2	53.9 ± 3.9
ΔG_{SA}	−5.8 ± 5.8	−5.8 ± 5.8	−5.9 ± 5.9	−5.8 ± 5.8	−5.9 ± 5.9	−5.7 ± 5.7	−5.6 ± 5.6	−5.4 ± 5.4	−6.1 ± 6.1	−5.7 ± 5.7	−5.8 ± 5.8
$\Delta E_{enthalpy}$	−55.6 ± 4.4	−55.1 ± 6.8	−55.1 ± 5.3	−55.7 ± 4.8	−56.4 ± 4.1	−56.9 ± 3.5	−55.2 ± 4.9	−52.8 ± 4.9	−58.3 ± 5.3	−55.4 ± 5.6	−53.4 ± 4.5
$-T\Delta S$	35.7 ± 4.1	36.0 ± 3.7	35.4 ± 3.5	35.2 ± 3.3	33.1 ± 4.1	32.0 ± 4.0	35.6 ± 3.9	33.1 ± 4.3	35.7 ± 4.1	34.8 ± 5.5	31.5 ± 4.6
$\Delta G_{binding}$	−19.8	−19.1	−19.7	−20.5	−23.3	−24.9	−19.6	−19.7	−22.6	−20.6	−21.9
$\Delta\Delta G_{binding}$ [a]	2.1	2.8	2.2	1.4	−1.4	−3.0	2.3	2.2	−0.7	1.3	0.0

[a] $\Delta\Delta G_{binding}(i) = \Delta G_{binding}(i) - \Delta G_{binding}$(apo-AR).

DOI: 10.1021/acs.jcim.8b00283
J. Chem. Inf. Model. XXXX, XXX, XXX−XXX

and communication between the coactivators and ARs. It should be noted that the binding free energies shown in Table 1 are only related to the interactions between the coactivator and ARs. Many other factors such as the ligand binding affinity would determine the AR activity, and therefore, $\Delta G_{binding}$ cannot match one-to-one with the quantitative values related to the AR activity, such as IC_{50} values.[55]

Single Mutations Affect the Ligand-Coactivator Allosteric Pathway. Many mutations on AR-LBD induce the resistance to the antiandrogen therapy of PCa. For instance, the antagonistic ligand hydroxyflutamide (HFT) was found to be an agonist to the T877A AR. The second-generation antiandrogen drug enzalutamide (MDV3100) displays an antagonistic capability on the WT-AR and T877A AR, but the F876L mutation confers resistance to MDV3100 both *in vitro* and *in vivo*.[20,29] On the other hand, as an AR inhibitor developed recently, ODM201 has shown its antagonistic effectivity on the T877A AR and F876L AR.[55]

In order to understand why a single mutation converts an AR ligand from antagonist to agonist, the effects of the T877A/F876L mutations on the structures of the AR bound with MDV3100 and ODM201 were studied. The results show that the binding of ODM201 would influence the AF-2 structures for both the F876L and T877A mutants of AR. The AF-2 RMSDs of the ODM201 bound F876L and T877A mutants are 3.8 and 4.0 Å, respectively. The AF-2 RMSD of the MDV3100 bound T877A mutant is 3.5 Å, which is comparable with that of the MDV3100 bound WT AR (3.7 Å). However, the AF-2 RMSD for the MDV3100 bound F876L mutant is 2.3 Å, suggesting there are no large structural changes on the AF-2 groove for the T877A mutant compared with the agonistic X-ray structure. Figure 7 gives the overlapped AF-2

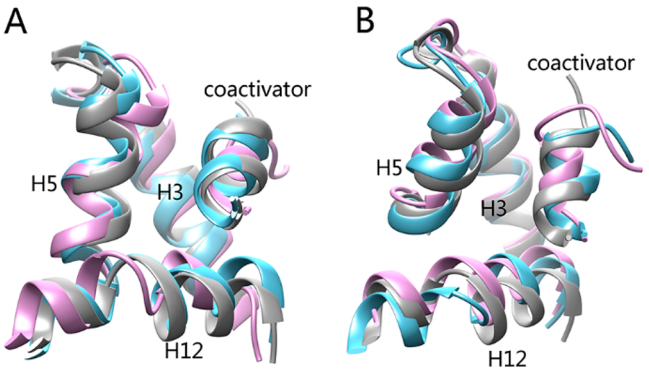

Figure 7. Structures of AF-2 bound with coactivator in the AR mutants. The conformations in the last 200 ns trajectories were classified into structure clusters based on the heavy-atom RMSDs. The AF-2 structures of the largest cluster center were selected as the representative structures. (A) Structure overlap of the MDV3100 bound T877A mutant (colored in magenta), MDV3100 bound F876L mutant (colored in cyan), and the X-ray structure (colored in gray). (B) Structure overlap of the ODM201 bound T877A mutant (colored in magenta), ODM201 bound F876L mutant (colored in cyan), and X-ray structure (colored in gray).

structures of the mutants to the agonistic experimental structure. It can be seen that the structure of the MDV3100 bound F876L mutant (colored in cyan in Figure 7A) is similar to the experimental structure, but the other mutants are distinct to the reference structure. In addition, the binding free energies of the coactivators in different AR mutants are consistent with their bioactivities, and the agonistic mutation F876L on the MDV3100 bound AR would reduce the binding free energy (Table 1).

Similar to the WT AR, the communications between the ligands and the coactivator in the mutated ARs are mediated by the H12−H4/H3-coactivator allosteric pathway. The mutations such as the F876L on the MDV3100 bound AR might change the interactions in the allosteric pathway and therefore convert the protein from the antagonistic state to the agonistic state. In the ligand binding pocket of the WT AR, MDV3100 was pushed toward to H12 by phenylalanine (F876) since the large volume of phenylalanine and, as a consequence, the methylene group in the middle of MDV3100 have the chance to contact the hydrophobic side chain of residue I899 on H12 (Figure 8A),

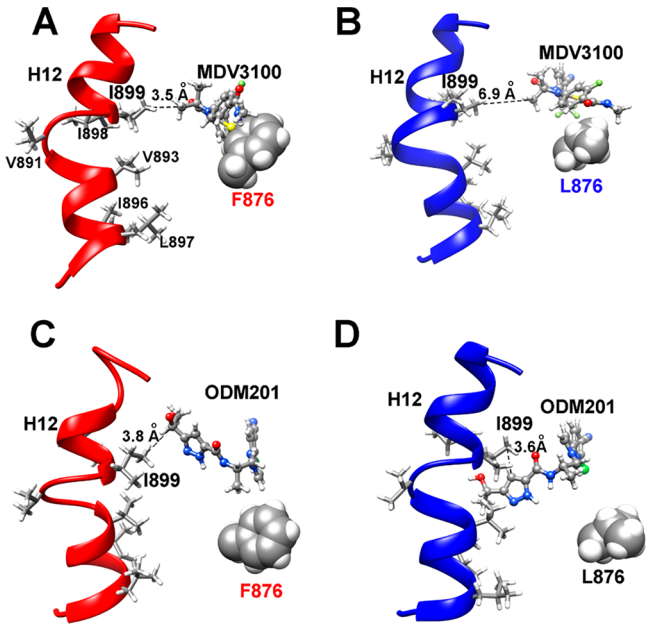

Figure 8. Regulation of the F876L mutation to the ligand-H12 interactions. (A) The WT AR bound with MDV3100. (B) The F876L AR mutant bound with MDV3100. (C) The WT AR bound with ODM201. (D) The F876L AR mutant bound with ODM201. The hydrophobic residues on H12 are shown as sticks and labeled. The side chain of residue 876 is shown as a sphere, and the ligands are represented as balls and sticks. The shortest distances between the heavy atoms on MDV3100 and I899 are given.

which would break the helical structure of H12 and induce the following allosteric interaction in the H12−H4/H3-coactivator pathway. Nevertheless, the tail of MDV3100 has greater space to move away from H12 if F876 is mutated to smaller residues such as leucine (Figure 8B), and the ligand would not damage the helical structure of H12 as well as the agonistic configuration of the AF-2 interface. For the ligand ODM201, the long tail guarantees the ligand always contacts H12, and the mutations on H10 (such as T877A and F876L) would not influence the contacts in the allosteric pathway. On the basis of the above observations, we conclude that large ligands with long tails have higher probability to avoid the drug tolerance induced by residue mutations on AR.

CONCLUSIONS

The communications between the AR-LBD and AR coactivator peptides are critical to the activation of AR. It is still unclear how the ligand binding would affect the AR-coactivator interactions. In this work, the MD simulations and MM/GBSA

DOI: 10.1021/acs.jcim.8b00283
J. Chem. Inf. Model. XXXX, XXX, XXX−XXX

calculations were used to study the structural basis of the ligand binding and the mutations to the AR-coactivator communications.

The structure differences between agonistic ARs (bound with DHT or HBP) and antagonistic ARs (bound with MDV3100, ODM201, ARN509, or ORM15341) as well as apo-AR were studied. The simulation results showed that the ligand binding mainly affects the structure of the function site AF-2, which consists of H3, H4, and H12. The ligands have some nontrivial effects on the overall scaffold of AF-2, and more importantly, the residue interactions in AF-2 are significantly regulated by the ligands. In addition, the interactions of several residues in the BF-3 interface, especially on the boundary of AF-2 and BF-3, are affected by the binding of ligands. The coactivator and AF-2 interactions follow a ligand−H12−H4/H3−coactivator allosteric pathway. The antagonistic ligands enhanced the binding free energy of the coactivator with AR-LBD, while the agonistic ligands weakened the binding free energy of AR-coactivator with AR-LBD.

The structural basis of the drug-tolerance induced by point mutations on AR was investigated. We found that the activity-related mutations would affect the AR-coactivator allosteric pathway. The F876L mutation converted the MDV3100 bound AR from antagonist to agonist by changing the orientation of the MDV3100 tail and the interactions between ligands and H12, and therefore, AF-2 in the mutant would convert to the agonistic configuration. The mechanism of how ligand-binding affects the AR-coactivator communications and the structural basis of drug-tolerance provided in this study would help to develop novel PCa drug candidates.

■ ASSOCIATED CONTENT

Supporting Information

The Supporting Information is available free of charge on the ACS Publications website at DOI: 10.1021/acs.jcim.8b00283.

Figure S1−S3, RMSD analysis of the MD trajectories; Figure S4, fragment average fraction of native contacts; Figure S5, fraction of native contacts of some important residues in different ligand bounded AR; Figure S6, sequence alignments of the ligand binding domain of nuclear receptors (PDF)

■ AUTHOR INFORMATION

Corresponding Authors

*Phone: +86-027-8719-7173. E-mail: mjduan@wipm.ac.cn.
*Phone: +86-517-8820-8412. E-mail: tingjunhou@zju.edu.cn.

ORCID

Huiyong Sun: 0000-0002-7107-7481
Mojie Duan: 0000-0002-5496-832X

Author Contributions

⊥These authors contribute equally to this work.

Notes

The authors declare no competing financial interest.

■ ACKNOWLEDGMENTS

This study was supported by National Major Basic Research Program of China (2016YFA0501701, 2016YFB0201700), National Science Foundation of China (21773298, 21403291, 21575128, 81603031), and National Institutes of Health of USA (R01-GM079383, R21-GM097617).

■ REFERENCES

(1) Gao, W.; Bohl, C. E.; Dalton, J. T. Chemistry and Structural Biology of Androgen Receptor. *Chem. Rev.* **2005**, *105*, 3352−3370.
(2) Heinlein, C. A.; Chang, C. Androgen Receptor in Prostate Cancer. *Endocr. Rev.* **2004**, *25*, 276−308.
(3) Debes, J. D.; Tindall, D. J. Mechanisms of Androgen-Refractory Prostate Cancer. *N. Engl. J. Med.* **2004**, *351*, 1488−1490.
(4) McCarthy, N. Prostate Cancer: Studying the Classics. *Nat. Rev. Cancer* **2011**, *11*, 386.
(5) Montgomery, R. B.; Mostaghel, E. A.; Vessella, R.; Hess, D. L.; Kalhorn, T. F.; Higano, C. S.; True, L. D.; Nelson, P. S. Maintenance of Intratumoral Androgens in Metastatic Prostate Cancer: A Mechanism for Castration-Resistant Tumor Growth. *Cancer Res.* **2008**, *68*, 4447−4454.
(6) Wong, Y. N.; Ferraldeschi, R.; Attard, G.; de Bono, J. Evolution of Androgen Receptor Targeted Therapy for Advanced Prostate Cancer. *Nat. Rev. Clin. Oncol.* **2014**, *11*, 365−376.
(7) Huang, P.; Chandra, V.; Rastinejad, F. Structural Overview of the Nuclear Receptor Superfamily: Insights into Physiology and Therapeutics. *Annu. Rev. Physiol.* **2010**, *72*, 247−272.
(8) Helsen, C.; Claessens, F. Looking at Nuclear Receptors from a New Angle. *Mol. Cell. Endocrinol.* **2014**, *382*, 97−106.
(9) van de Wijngaart, D. J.; Dubbink, H. J.; van Royen, M. E.; Trapman, J.; Jenster, G. Androgen Receptor Coregulators: Recruitment Via the Coactivator Binding Groove. *Mol. Cell. Endocrinol.* **2012**, *352*, 57−69.
(10) van de Wijngaart, D. J.; van Royen, M. E.; Hersmus, R.; Pike, A. C.; Houtsmuller, A. B.; Jenster, G.; Trapman, J.; Dubbink, H. J. Novel Fxxff and Fxxmf Motifs in Androgen Receptor Cofactors Mediate High Affinity and Specific Interactions with the Ligand-Binding Domain. *J. Biol. Chem.* **2006**, *281*, 19407−19416.
(11) van de Wijngaart, D. J.; Dubbink, H. J.; Molier, M.; de Vos, C.; Trapman, J.; Jenster, G. Functional Screening of Fxxlf-Like Peptide Motifs Identifies Smarcd1/Baf60a as an Androgen Receptor Cofactor That Modulates Tmprss2 Expression. *Mol. Endocrinol.* **2009**, *23*, 1776−1786.
(12) Hsu, C. L.; Chen, Y. L.; Ting, H. J.; Lin, W. J.; Yang, Z.; Zhang, Y.; Wang, L.; Wu, C. T.; Chang, H. C.; Yeh, S.; Pimplikar, S. W.; Chang, C. Androgen Receptor (Ar) Nh2- and Cooh-Terminal Interactions Result in the Differential Influences on the Ar-Mediated Transactivation and Cell Growth. *Mol. Endocrinol.* **2005**, *19*, 350−361.
(13) van de Wijngaart, D. J.; Dubbink, H. J.; Molier, M.; de Vos, C.; Jenster, G.; Trapman, J. Inhibition of Androgen Receptor Functions by Gelsolin Fxxff Peptide Delivered by Transfection, Cell-Penetrating Peptides, and Lentiviral Infection. *Prostate* **2011**, *71*, 241−253.
(14) Bennett, N. C.; Gardiner, R. A.; Hooper, J. D.; Johnson, D. W.; Gobe, G. C. Molecular Cell Biology of Androgen Receptor Signalling. *Int. J. Biochem. Cell Biol.* **2010**, *42*, 813−827.
(15) Shang, Y.; Myers, M.; Brown, M. Formation of the Androgen Receptor Transcription Complex. *Mol. Cell* **2002**, *9*, 601−610.
(16) He, B.; Kemppainen, J. A.; Voegel, J. J.; Gronemeyer, H.; Wilson, E. M. Activation Function 2 in the Human Androgen Receptor Ligand Binding Domain Mediates Interdomain Communication with the Nh(2)-Terminal Domain. *J. Biol. Chem.* **1999**, *274*, 37219−37225.
(17) Pienta, K. J.; Bradley, D. Mechanisms Underlying the Development of Androgen-Independent Prostate Cancer. *Clin. Cancer Res.* **2006**, *12*, 1665−1671.
(18) Matsumoto, T.; Sakari, M.; Okada, M.; Yokoyama, A.; Takahashi, S.; Kouzmenko, A.; Kato, S. The Androgen Receptor in Health and Disease. *Annu. Rev. Physiol.* **2013**, *75*, 201−224.
(19) Mateo, J.; Smith, A.; Ong, M.; de Bono, J. S. Novel Drugs Targeting the Androgen Receptor Pathway in Prostate Cancer. *Cancer Metastasis Rev.* **2014**, *33*, 567−579.
(20) Balbas, M. D.; Evans, M. J.; Hosfield, D. J.; Wongvipat, J.; Arora, V. K.; Watson, P. A.; Chen, Y.; Greene, G. L.; Shen, Y.; Sawyers, C. L. Overcoming Mutation-Based Resistance to Antian-

DOI: 10.1021/acs.jcim.8b00283
J. Chem. Inf. Model. XXXX, XXX, XXX−XXX

drogens with Rational Drug Design. *eLife* **2013**, *2*, No. e00499, DOI: 10.7554/eLife.00499.
(21) Tran, C.; Ouk, S.; Clegg, N. J.; Chen, Y.; Watson, P. A.; Arora, V.; Wongvipat, J.; Smith-Jones, P. M.; Yoo, D.; Kwon, A.; Wasielewska, T.; Welsbie, D.; Chen, C. D.; Higano, C. S.; Beer, T. M.; Hung, D. T.; Scher, H. I.; Jung, M. E.; Sawyers, C. L. Development of a Second-Generation Antiandrogen for Treatment of Advanced Prostate Cancer. *Science* **2009**, *324*, 787−790.
(22) Elhaji, Y. A.; Stoica, I.; Dennis, S.; Purisima, E. O.; Trifiro, M. A. Impaired Helix 12 Dynamics Due to Proline 892 Substitutions in the Androgen Receptor Are Associated with Complete Androgen Insensitivity. *Hum. Mol. Genet.* **2006**, *15*, 921−931.
(23) Zhou, J.; Liu, B.; Geng, G.; Wu, J. H. Study of the Impact of the T877a Mutation on Ligand-Induced Helix-12 Positioning of the Androgen Receptor Resulted in Design and Synthesis of Novel Antiandrogens. *Proteins: Struct., Funct., Genet.* **2010**, *78*, 623−637.
(24) Nagata, N.; Kawai, K.; Nakanishi, I. Subtle Structural Changes in Tetrahydroquinolines, a New Class of Nonsteroidal Selective Androgen Receptor Modulators, Induce Different Functions. *J. Chem. Inf. Model.* **2012**, *52*, 2257−2264.
(25) Duan, M.; Liu, N.; Zhou, W.; Li, D.; Yang, M.; Hou, T. Structural Diversity of Ligand-Binding Androgen Receptors Revealed by Microsecond Long Molecular Dynamics Simulations and Enhanced Sampling. *J. Chem. Theory Comput.* **2016**, *12*, 4611−4619.
(26) Kattoula, S. R.; Baker, M. E. Structural and Evolutionary Analysis of the Co-Activator Binding Domain in Vertebrate Progesterone Receptors. *J. Steroid Biochem. Mol. Biol.* **2014**, *141*, 7−15.
(27) Estebanez-Perpina, E.; Arnold, L. A.; Nguyen, P.; Rodrigues, E. D.; Mar, E.; Bateman, R.; Pallai, P.; Shokat, K. M.; Baxter, J. D.; Guy, R. K.; Webb, P.; Fletterick, R. J. A Surface on the Androgen Receptor That Allosterically Regulates Coactivator Binding. *Proc. Natl. Acad. Sci. U. S. A.* **2007**, *104*, 16074−16079.
(28) Grosdidier, S.; Carbo, L. R.; Buzon, V.; Brooke, G.; Nguyen, P.; Baxter, J. D.; Bevan, C.; Webb, P.; Estebanez-Perpina, E.; Fernandez-Recio, J. Allosteric Conversation in the Androgen Receptor Ligand-Binding Domain Surfaces. *Mol. Endocrinol.* **2012**, *26*, 1078−1090.
(29) Korpal, M.; Korn, J. M.; Gao, X.; Rakiec, D. P.; Ruddy, D. A.; Doshi, S.; Yuan, J.; Kovats, S. G.; Kim, S.; Cooke, V. G.; Monahan, J. E.; Stegmeier, F.; Roberts, T. M.; Sellers, W. R.; Zhou, W.; Zhu, P. An F876l Mutation in Androgen Receptor Confers Genetic and Phenotypic Resistance to Mdv3100 (Enzalutamide). *Cancer Discovery* **2013**, *3*, 1030−1043.
(30) Prekovic, S.; van Royen, M. E.; Voet, A. R.; Geverts, B.; Houtman, R.; Melchers, D.; Zhang, K. Y.; Van den Broeck, T.; Smeets, E.; Spans, L.; Houtsmuller, A. B.; Joniau, S.; Claessens, F.; Helsen, C. The Effect of F877l and T878a Mutations on Androgen Receptor Response to Enzalutamide. *Mol. Cancer Ther.* **2016**, *15*, 1702−1712.
(31) Xu, X.; Yang, W.; Wang, X.; Li, Y.; Wang, Y.; Ai, C. Dynamic Communication between Androgen and Coactivator: Mutually Induced Conformational Perturbations in Androgen Receptor Ligand-Binding Domain. *Proteins: Struct., Funct., Genet.* **2011**, *79*, 1154−1171.
(32) Osguthorpe, D. J.; Hagler, A. T. Mechanism of Androgen Receptor Antagonism by Bicalutamide in the Treatment of Prostate Cancer. *Biochemistry* **2011**, *50*, 4105−4113.
(33) Liu, H.; Wang, L.; Tian, J.; Li, J.; Liu, H. Molecular Dynamics Studies on the Enzalutamide Resistance Mechanisms Induced by Androgen Receptor Mutations. *J. Cell. Biochem.* **2017**, *118*, 2792−2801.
(34) Nique, F.; Hebbe, S.; Peixoto, C.; Annoot, D.; Lefrancois, J. M.; Duval, E.; Michoux, L.; Triballeau, N.; Lemoullec, J. M.; Mollat, P.; Thauvin, M.; Prange, T.; Minet, D.; Clement-Lacroix, P.; Robin-Jagerschmidt, C.; Fleury, D.; Guedin, D.; Deprez, P. Discovery of Diarylhydantoins as New Selective Androgen Receptor Modulators. *J. Med. Chem.* **2012**, *55*, 8225−8235.
(35) Friesner, R. A.; Banks, J. L.; Murphy, R. B.; Halgren, T. A.; Klicic, J. J.; Mainz, D. T.; Repasky, M. P.; Knoll, E. H.; Shelley, M.; Perry, J. K.; Shaw, D. E.; Francis, P.; Shenkin, P. S. Glide: A New Approach for Rapid, Accurate Docking and Scoring. 1. Method and Assessment of Docking Accuracy. *J. Med. Chem.* **2004**, *47*, 1739−1749.
(36) Madhavi Sastry, G.; Adzhigirey, M.; Day, T.; Annabhimoju, R.; Sherman, W. Protein and Ligand Preparation: Parameters, Protocols, and Influence on Virtual Screening Enrichments. *J. Comput.-Aided Mol. Des.* **2013**, *27*, 221−234.
(37) Lindorff-Larsen, K.; Piana, S.; Palmo, K.; Maragakis, P.; Klepeis, J. L.; Dror, R. O.; Shaw, D. E. Improved Side-Chain Torsion Potentials for the Amber Ff99sb Protein Force Field. *Proteins: Struct., Funct., Genet.* **2010**, *78*, 1950−1958.
(38) Wang, J.; Wolf, R. M.; Caldwell, J. W.; Kollman, P. A.; Case, D. A. Development and Testing of a General Amber Force Field. *J. Comput. Chem.* **2004**, *25*, 1157−1174.
(39) Essmann, U.; Perera, L.; Berkowitz, M. L.; Darden, T.; Lee, H.; Pedersen, L. G. A Smooth Particle Mesh Ewald Method. *J. Chem. Phys.* **1995**, *103*, 8577.
(40) Loncharich, R. J.; Brooks, B. R.; Pastor, R. W. Langevin Dynamics of Peptides: The Frictional Dependence of Isomerization Rates of N-Acetylalanyl-N'-Methylamide. *Biopolymers* **1992**, *32*, 523−535.
(41) Gotz, A. W.; Williamson, M. J.; Xu, D.; Poole, D.; Le Grand, S.; Walker, R. C. Routine Microsecond Molecular Dynamics Simulations with Amber on Gpus. 1. Generalized Born. *J. Chem. Theory Comput.* **2012**, *8*, 1542−1555.
(42) Lambrakos, S.; Boris, J.; Oran, E.; Chandrasekhar, I.; Nagumo, M. A Modified Shake Algorithm for Maintaining Rigid Bonds in Molecular Dynamics Simulations of Large Molecules. *J. Comput. Phys.* **1989**, *85*, 473−486.
(43) Best, R. B.; Hummer, G.; Eaton, W. A. Native Contacts Determine Protein Folding Mechanisms in Atomistic Simulations. *Proc. Natl. Acad. Sci. U. S. A.* **2013**, *110*, 17874−17879.
(44) Duan, M.; Liu, H.; Li, M.; Huo, S. Network Representation of Conformational Transitions between Hidden Intermediates of Rd-Apocytochrome B562. *J. Chem. Phys.* **2015**, *143*, 135101.
(45) Kollman, P. A.; Massova, I.; Reyes, C.; Kuhn, B.; Huo, S.; Chong, L.; Lee, M.; Lee, T.; Duan, Y.; Wang, W.; Donini, O.; Cieplak, P.; Srinivasan, J.; Case, D. A.; Cheatham, T. E., 3rd Calculating Structures and Free Energies of Complex Molecules: Combining Molecular Mechanics and Continuum Models. *Acc. Chem. Res.* **2000**, *33*, 889−897.
(46) Weiser, J.; Shenkin, P. S.; Still, W. C. Approximate Solvent-Accessible Surface Areas from Tetrahedrally Directed Neighbor Densities. *Biopolymers* **1999**, *50*, 373−380.
(47) Onufriev, A.; Bashford, D.; Case, D. A. Exploring Protein Native States and Large-Scale Conformational Changes with a Modified Generalized Born Model. *Proteins: Struct., Funct., Genet.* **2004**, *55*, 383−394.
(48) Miller, B. R., 3rd; McGee, T. D., Jr.; Swails, J. M.; Homeyer, N.; Gohlke, H.; Roitberg, A. E. Mmpbsa.Py: An Efficient Program for End-State Free Energy Calculations. *J. Chem. Theory Comput.* **2012**, *8*, 3314−3321.
(49) Gunther, J. R.; Du, Y.; Rhoden, E.; Lewis, I.; Revennaugh, B.; Moore, T. W.; Kim, S. H.; Dingledine, R.; Fu, H.; Katzenellenbogen, J. A. A Set of Time-Resolved Fluorescence Resonance Energy Transfer Assays for the Discovery of Inhibitors of Estrogen Receptor-Coactivator Binding. *J. Biomol. Screening* **2009**, *14*, 181−193.
(50) Nandhikonda, P.; Lynt, W. Z.; McCallum, M. M.; Ara, T.; Baranowski, A. M.; Yuan, N. Y.; Pearson, D.; Bikle, D. D.; Guy, R. K.; Arnold, L. A. Discovery of the First Irreversible Small Molecule Inhibitors of the Interaction between the Vitamin D Receptor and Coactivators. *J. Med. Chem.* **2012**, *55*, 4640−4651.
(51) He, B.; Gampe, R. T., Jr.; Kole, A. J.; Hnat, A. T.; Stanley, T. B.; An, G.; Stewart, E. L.; Kalman, R. I.; Minges, J. T.; Wilson, E. M. Structural Basis for Androgen Receptor Interdomain and Coactivator Interactions Suggests a Transition in Nuclear Receptor Activation Function Dominance. *Mol. Cell* **2004**, *16*, 425−438.

DOI: 10.1021/acs.jcim.8b00283
J. Chem. Inf. Model. XXXX, XXX, XXX−XXX

(52) He, B.; Minges, J. T.; Lee, L. W.; Wilson, E. M. The Fxxlf Motif Mediates Androgen Receptor-Specific Interactions with Coregulators. *J. Biol. Chem.* **2002**, *277*, 10226−10235.
(53) Zhang, Y.; Mantravadi, P. K.; Jobbagy, S.; Bao, W.; Koh, J. T. Antagonizing the Androgen Receptor with a Biomimetic Acyltransferase. *ACS Chem. Biol.* **2016**, *11*, 2797−2802.
(54) Buzon, V.; Carbo, L. R.; Estruch, S. B.; Fletterick, R. J.; Estebanez-Perpina, E. A Conserved Surface on the Ligand Binding Domain of Nuclear Receptors for Allosteric Control. *Mol. Cell. Endocrinol.* **2012**, *348*, 394−402.
(55) Moilanen, A. M.; Riikonen, R.; Oksala, R.; Ravanti, L.; Aho, E.; Wohlfahrt, G.; Nykanen, P. S.; Tormakangas, O. P.; Palvimo, J. J.; Kallio, P. J. Discovery of Odm-201, a New-Generation Androgen Receptor Inhibitor Targeting Resistance Mechanisms to Androgen Signaling-Directed Prostate Cancer Therapies. *Sci. Rep.* **2015**, *5*, 12007.

DOI: 10.1021/acs.jcim.8b00283
J. Chem. Inf. Model. XXXX, XXX, XXX−XXX